Lab on a Chip

Dynamic Article Links

Cite this: *Lab Chip*, 2011, **11**, 2231

www.rsc.org/loc

PAPER

A new micropatterning method of soft substrates reveals that different tumorigenic signals can promote or reduce cell contraction levels†

Qingzong Tseng,[a] Irene Wang,[b] Eve Duchemin-Pelletier,[c] Ammar Azioune,[d] Nicolas Carpi,[d] Jie Gao,[b] Odile Filhol,[c] Matthieu Piel,[d] Manuel Théry*[a] and Martial Balland*[b]

Received 29th November 2010, Accepted 6th April 2011
DOI: 10.1039/c0lc00641f

In tissues, cell microenvironment geometry and mechanics strongly impact on cell physiology. Surface micropatterning allows the control of geometry while deformable substrates of tunable stiffness are well suited for the control of the mechanics. We developed a new method to micropattern extracellular matrix proteins on poly-acrylamide gels in order to simultaneously control cell geometry and mechanics. Microenvironment geometry and mechanics impinge on cell functions by regulating the development of intra-cellular forces. We measured these forces in micropatterned cells. Micropattern geometry was streamlined to orient forces and place cells in comparable conditions. Thereby force measurement method could be simplified and applied to large-scale experiment on chip. We applied this method to mammary epithelial cells with traction force measurements in various conditions to mimic tumoral transformation. We found that, contrary to the current view, all transformation phenotypes were not always associated to an increased level of cell contractility.

Introduction

Geometrical and mechanical properties of cell microenvironments have a profound impact on cell morphogenesis and functions. They will impinge on cell cytoskeleton architecture, polarity, migration, division, growth, and differentiation.[1] New materials have been engineered to reveal these effects, investigate the mechanisms by which they regulate cell functions and eventually control them to design new tools for tissue engineering applications. Microenvironment geometry has been controlled with micro-patterning techniques. They were used to manipulate the localization of adhesive molecules from the extracellular matrix (ECM) and thereby control the position and shape of individual cells.[2] Microenvironment mechanics have been controlled with soft substrates. The reticulation and density of synthetic or bio-polymers were used to control their stiffness.[3,4] Both parameters, geometry and mechanics, should be controlled on the same material to faithfully reproduce the physiological conditions that cells encounter in tissues and to fully control the physical signals affecting cell morphogenesis. Cell shape control on deformable substrates has been performed using various micro-fabricated tools on either poly-acrylamide (PA) gels or arrays of micro-pillars. Micro-molded stamps,[5] stencils[6,7] or microfluidic channels[8] were used to locally deposit ECM proteins on chemically activated PA. Micro-contact printing was used to print ECM proteins on arrays of micro-pillars.[9] We developed a new, fast, efficient and robust micropatterning method on PA in which no specific microfabricated tool was required except the commercially available photomask. We validated it by controlling the shape, cytoskeleton architecture and traction force production of human mammary epithelial cells.

Microenvironment geometry and mechanics affect cell architecture and function notably by modulating the forces produced by cells. Cells attach to their microenvironment and exert traction forces *via* the myosin dependent contraction of their actin cytoskeleton. Microenvironment geometry will affect the orientation of contractile stress fibers and the location of force application sites (Fig. S1†). In spatially confined, non-migrating cells, stress fibers form along cell edges resulting in the application of traction forces at cell apices.[6,7] Stress fibers appear larger when no ECM is available for cell adhesion between cell apices.[10] Microenvironment stiffness will affect the magnitude of cell traction forces: a stiffer substrate will promote larger forces.[11,12] The sub-cellular location of traction forces affects intra-cellular organization, notably centrosome positioning,[13] primary cilium growth[14] and intra-cellular trafficking.[15] It is therefore a major regulator of cell polarity.[16] Cell contractility also governs

[a]*Laboratoire de Physiologie Cellulaire et Végétale, iRTSV, CEA/CNRS/UJF/INRA, 17 rue des martyrs, 38054 Grenoble, France. E-mail: manuel.thery@cea.fr*
[b]*Laboratoire de Spectrométrie Physique, CNRS/UJF, UMR5588, 140 Avenue de la Physique, 38402 Saint Martin d'Heres, France. E-mail: martial.balland@ujf-grenoble.fr*
[c]*Laboratoire de Transduction du Signal, iRTSV, CEA/CNRS/UJF, 17 rue des martyrs, 38054 Grenoble, France*
[d]*Institut Curie, CNRS UMR 144, 26 rue d'Ulm, 75248 Paris Cedex 05, France*
† Electronic supplementary information (ESI) available. See DOI: 10.1039/c0lc00641f

extensive cytoskeletal remodeling during cell migration,[17,18] and division.[19] In addition, cell contractility promotes cell growth[20] and directs stem cell differentiation.[11] Considering this broad impact of actin cytoskeleton contractility on cell physiology, it is not surprising that up-regulation of force production is involved in tumoral transformation.[21,22] Polarity misorientation,[14] disordered cell positioning[23,24] and amplified growth[25] are characteristic tumoral features that can be induced by increasing cell contractility. Therefore, Rho kinase inhibitors, which reduce the level of cell contractility, have been seriously considered as cancer treatment agents.[26,27] However, many pathways lead to tumoral transformation and it is not clear yet whether high levels of cell contraction are systematically associated to tumoral transformation. To investigate this issue, we took advantage of our new micropatterning method of PA to orient cell traction forces and impose them to perform a standardized exercise. With identical spreading and location of stress fibers, cells were rigorously and easily comparable to each other. We could quantify the effect of various tumorigenic treatments on human mammary epithelial cells.

Results

New micropatterning method on soft substrate

We used direct exposure of PA to deep UV (180 nm) through an optical quartz mask to rapidly achieve micropatterning, with high spatial resolution and reproducibility, on a soft substrate of controlled stiffness (see Experimental section). A drop of acrylamide solution was placed directly on the chromium side of the

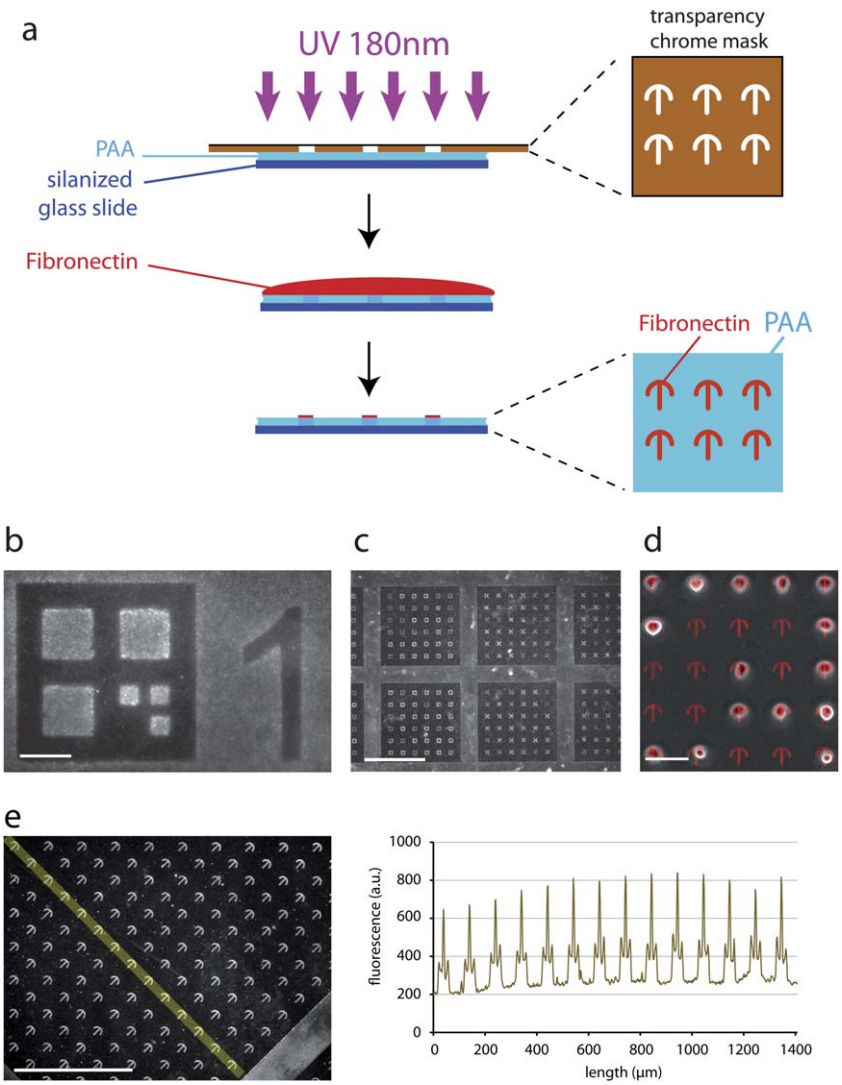

Fig. 1 Micropatterning of PA gel. (a) PA micropatterning method. The gel is polymerized on the photomask, exposed to deep UV and coated with ECM proteins. Cells attach specifically to the UV exposed regions. (b) Fibronectin and fibrinogen-A546 coating on micropatterned PA. Scale bar represents 10 μm. (c) Fibronectin and fibrinogen-A546 coating on micropatterned PA. Scale bar represents 500 μm. (d) MCF10A cells (phase contrast) plated on crossbow shaped micropattern (red) on PA. Cells specifically attach on the micropatterns. Scale bar represents 100 μm. (e) Linescan of fluorescence intensity along a 1 mm long line (yellow) showing the homogeneity of fluorescence staining and reproducibility of micropattern shapes. Scale bar represents 500 μm.

optical mask and covered with a silanized glass coverslip. After PA polymerization, the sandwich was exposed to deep UV through the micropatterned transparent regions of the optical mask. Deep UVs generate ozone which activate the PA[28–30] (Fig. 1a). The coverslip along with the PA gel was removed from the mask and coated with crosslinker and fibronectin, which adsorbed only on the UV-exposed regions. The direct contact with the optical mask during PA polymerization and UV-exposure allowed a faithful reproduction of its spatial features and ensured a good, sub-cellular, spatial resolution. 3 micron wide squares, corresponding to the minimum size we could obtain on low cost quartz mask, could be resolved on PA (Fig. 1b). The coating was quite homogeneous over the entire coverslip (Fig. 1c and e). The entire process, from PA preparation to the end of protein coating, lasts 2 h, including 1 h of PA polymerization.

Controlled localisation and focusing of force application sites

Non-tumorigenic human epithelial cells from the mammary gland, MCF10A, were plated on the micropatterned PA substrates. Cells specifically attached to the fibronectin coated micropatterns since non-exposed PA regions prevented protein adsorption (Fig. 1d). The effect of micropattern geometry on the orientation of cell traction forces was tested on various shapes: disc, pacman and crossbow (Fig. 2a). Spread cells exerted traction forces on the micropattern that could be measured by looking at the displacement of fluorescent beads embedded in the PA gel (see Fig. 2b and Experimental section). Particle image velocimetry followed by individual particle tracking were used to measure bead displacements.[31,32] Force fields were calculated from the bead displacement fields using the Fourier transform traction cytometry.[32,33] Force fields exerted by individual cells were overlaid and averaged to quantify their reproducibility (Fig. 2c and d). On homogeneously coated regions cells developed forces that were randomly distributed from one cell to the other. In cells constrained on disc shaped micropatterns, forces were still randomly oriented but their magnitudes were lowered due to reduced cell spreading.[9] In cells constrained on pacman shaped micropatterns, force distribution was geometrically biased due to enhanced cell contraction above non adhesive regions.[10] Cell ability to exert traction forces was even more stimulated on crossbow shaped micropatterns, where the total traction force per cell was higher than on any other micropattern shape (Fig. 2d and S2†). Importantly, most of the traction forces were reproducibly oriented upward, along the straight adhesive bar, on the extremity of which we measured the highest pressure (Fig. 2d and S3†). These results demonstrated that appropriate micropattern geometries can both stimulate cell contraction and orient force application. Such geometries place cells in optimal conditions to reveal potential cell contractility and measure their contraction strength.

Force field streamlining allows reproducible force-deformation relationship

Cells deform the soft micropattern when pulling on it. The local amplitude of the deformation is related to the local force application. However, when all actin cables are oriented toward a single point, as it is the case on crossbow shaped micropatterns (Fig. S1†), the local deformation could reveal the total amount of contractile forces. If so a very simple measurement of the local deformation could be a simple and direct measure of the global cell contraction level. Such a measure would be convenient for high throughput and large-scale analyses. To test this hypothesis, we used classical force field calculations with beads embedded in the PA gel (Fig. 2b) and observation of micropattern deformation (Fig. 3a) to establish the force–deformation relationship in micropatterned cells. On discs the deformation orientation was unpredictable and no good correlation could be found between the deformation along a reference axis and the total cell traction force (Fig. 3b). When the deformation was measured along the shortest, and therefore most contracted, cell axis, the correlation was improved (Fig. 3c). However this shape did not stimulate cell contraction and therefore did not fully reveal a cell contractility potential (Fig. 2d and S2†). Cell traction force magnitudes were slightly higher on pacman shapes, but force and deformation were not precisely correlated (Fig. 3d). On the crossbow, the length of the straight bar is compressed in response to oriented cell traction forces (Fig. 3a and S3†). We found a good linear correlation between crossbow bar shortening, a local measure, and total cell traction, a global cell state (Fig. 3e). Each length variation could be assigned to a defined force value. This revealed that crossbow bar length could be taken as a direct indicator of cell contraction level.

On the crossbow, a single image acquisition was sufficient to measure the bar length and read the corresponding total cell traction force using the calibration curve (Fig. 3f). It was no longer necessary to track beads in the substrate and detach the cell to recover the original bead positions in order to obtain the same measurement. Global force measurement was not only easier compared to any previous method but it also became amenable to automation.

We tested whether this linear relationship was also valid for other rigidities than the 7 kPa gels used throughout this study. On softer gels, below the range of 3 kPa, the micropattern geometry was less reproducible (Fig. S4†). So force measurements at this rigidity could not be reliably performed. With harder gels (14 kPa), the linear relationship was preserved. However, those higher rigidities naturally lead to smaller gel deformations. Thus in order to maximize the signal to noise ratio in length measurements, gels of 7 kPa were optimal, in the case of MCF10A cells, to allow reliable force measurement based on micropattern deformation.

Validation of force measurement

We validated this methodology by analyzing the well-described blebbistatin effects on cell contractility. Blebbistatin has been shown to inhibit myosin-II ATPase.[34] Cells were treated with an increasing dose of blebbistatin (Movie S1†). Crossbow bar length measurements on thresholded pictures of the fluorescent micropattern were used to estimate cell traction forces (Fig. 4a). The force inhibition profile in response to increasing dose of blebbistatin matched the myosin II inhibition profile[34] and the cellular force profile measured with other techniques.[35] Drug effects on cell contractility could thus easily and rapidly be quantified using this new methodology.

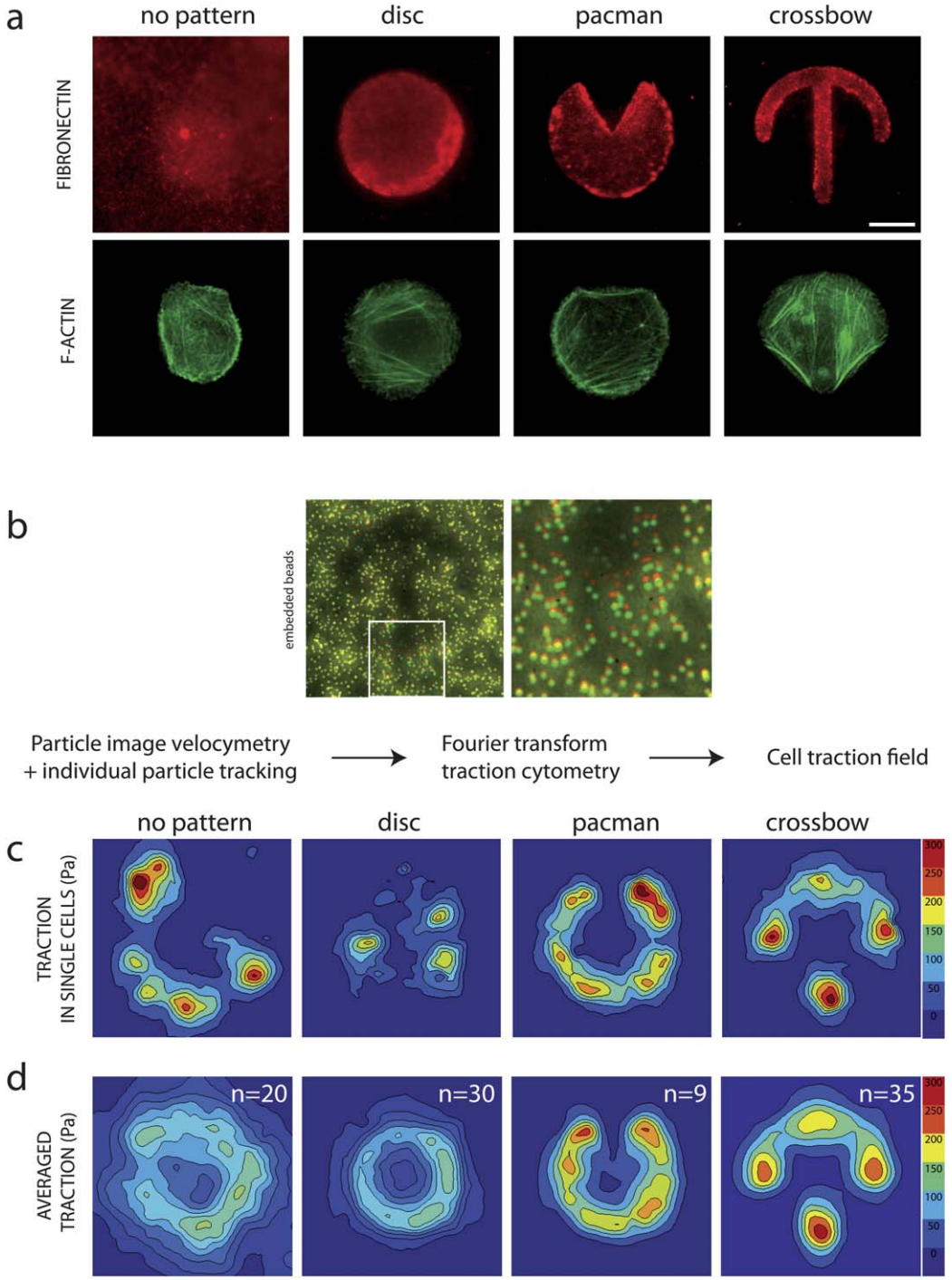

Fig. 2 Actin cytoskeleton streamlining normalizes the cell traction force field. (a) Micropattern geometry orients actin network architecture. Individual MCF10A cells plated either on non-patterned, fibronectin coated, glass slide, or on disc, pacman or crossbow shaped fibronectin micropatterns (red). Cells were fixed and stained with phalloidin to reveal F-actin filaments (green). Cells preferentially form contractile F-actin bundles, or stress fibers, above non-adhesive regions. Scale bar represents 10 μm. (b) Gel embedded beads were used to calculate the cell traction force with Fourier transform traction cytometry. Pictures of the beads were taken before (red) and after (green) cell detachment with trypsin to visualize the gel deformation upon the cell traction forces. Bead displacement was automatically detected and processed to infer the corresponding traction force field (see Experimental). (c) Traction force field calculations show that the cell exhibits an unpredictable spatial distribution of stress in non-patterned and in disc-shaped patterned cells. Cells patterned on pacman, and crossbow, develop enhanced traction forces on adhesion sites flanking non-adhesive regions. (d) Overlaying and averaging of traction force fields highlight the variability of traction force fields in non patterned cells. Non patterned cells were aligned using their nucleus position. Force fields were more precisely quantified in micropatterned cells. Crossbow shaped micropatterns reproducibly concentrate the location of cell traction forces in the bottom part of the vertical bar. Scale bar is 10 μm. Traction magnitude corresponds to the local force per area unit so it is given in Pascals.

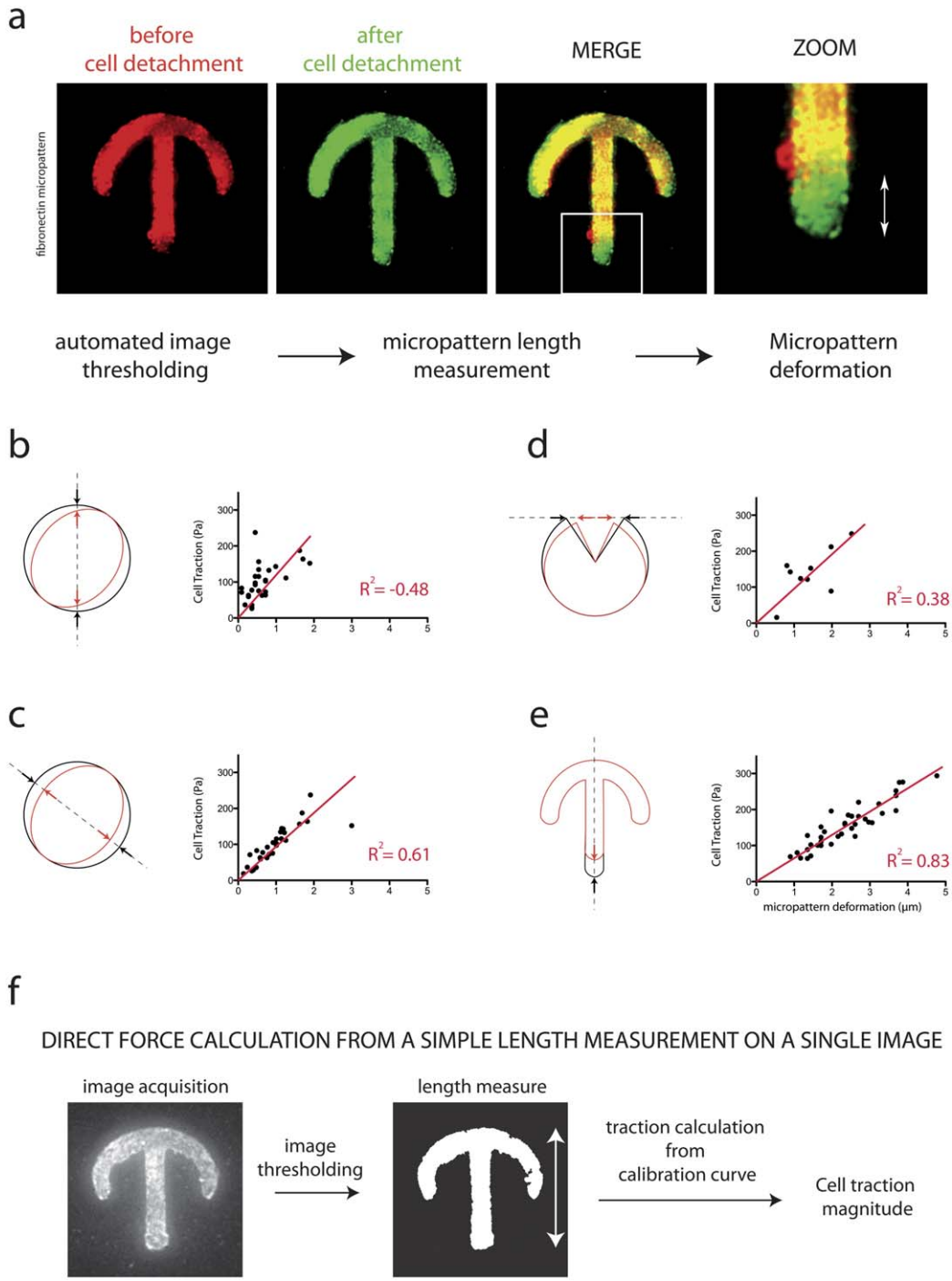

Fig. 3 Simple measurement of micropattern deformation allows easy, fast and accurate force quantification. (a) Fibrinogen-Alexa 546 coating was used to measure micropattern deformation. Pictures of micropatterns were taken before (red) and after (green) cell detachment with trypsin to visualize the micropattern deformation from the cell traction forces. (b) Red and black drawings represent micropattern shape before and after cell detachment. The micropattern deformation length corresponded to the distance between the red and black arrows. Micropattern deformation was then plotted against the total traction force exerted by the cell (normalized by cell area). Data points were fitted with a linear regression (full line). On discs, micropattern deformation could not be predicted. It was measured along an arbitrary vertical axis. The correlation in this case between total traction and micropattern deformation was not good. (c) The correlation was better when disc deformation was measured along the axis displaying the largest deformation. (d) On pacman shaped micropatterns the correlation was not optimal since the deformation was quite small and associated to large errors. (e) On crossbow shaped micropatterns the total cell traction force could be directly correlated to the micropattern deformation with a small deviation from the linear fit. This calibration curve was used in the following experiments. (f) New methodology to measure cell traction forces without bead displacement measurements or inverse problem calculation.

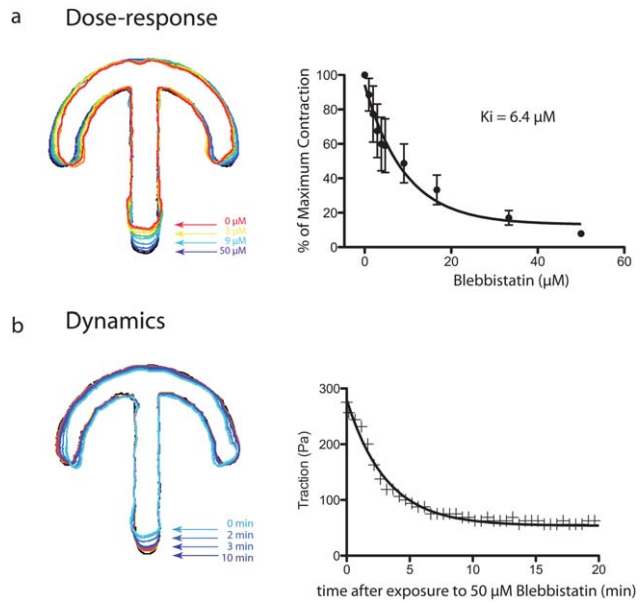

Fig. 4 Validation of simplified force measurements in response to myosin inactivation treatment. (a) Cell traction forces in response to blebbistatin, calculated by the method illustrated in Fig. 3f. Increasing drug concentrations were successively applied to 6 cells. Colored micropattern contours show a representative micropattern relaxation upon increasing drug concentrations. In the graph, the maximal cell tractions in the absence of blebbistatin were renormalized. Error bars represent the standard deviation. Data were fitted with a single exponential decay (full line) to calculate the IC50, *i.e.* drug concentration for half effect. (b) Cell traction forces over time in response to 50 µM of blebbistatin, calculated by the method illustrated in Fig. 3f. Colored micropattern contours show a representative micropattern relaxation over time. Measurements were performed on a single cell. Data were fitted with a single exponential decay (full line).

In addition we tested this new method for another application requiring numerous, and thus fast, force measurements: the analysis of force relaxation over time. We measured the force magnitude decrease in response to 50 µM of blebbistatin and found that it follows a single exponential decay (Fig. 4b).

All tumorigenic transformation do not increase cell contractility

We then used our method to compare the contraction level of wild type (WT) MCF10A cells *versus* drug treated or genetically modified MCF10A cells mimicking various forms of tumoral transformation. Indeed, tumor transformation has been shown to be associated with high levels of cell contraction.[21] This suggested that cell contraction level measurements could help in the diagnosis of cancer progression and allow the development of new and improved treatments.[36] We tested various treatments known to induce cell behaviors mimicking tumoral transformation: cell exposure to transforming growth factor beta 1 (TGFβ),[37] ErbB2 receptor activation,[38] and Protein kinase CK2 (previously known as Casein Kinase 2) inactivation.[39–43] Although already well characterized, their effect on the induction of a tumoral-like phenotype was tested here on MCF10A cells. We made two characteristic tests of tumoral-like behaviors: anchorage-independent growth[44,45] and inability to self-assemble into acini-like structures in 3D matrix.[46,47] Anchorage dependency for cell growth was tested by plating cells on soft agar.[44] Wild type MCF10A died, as revealed by the presence of black cell phantom (Fig. 5a). Inactivation of the beta subunit of CK2 as well as activation of ErbB2 receptors promoted cell growth. TGFβ treatment allowed cells to aggregate and survive (Fig. 5a). The ability to self-assemble into a mammary acini-like structure was tested by cultivating cells in Matrigel.[48] After one week, the wild type MCF10A formed the expected hollow spheres, as revealed by the reduction of nuclei in the central part of the structure (Fig. 5b). In all other conditions, cells formed irregular structures without cell clearance in the central part (Fig. 5b). These two analyses clearly confirmed that the three treatments conferred tumoral features to MCF10A cells.

MCF10A cells were treated for 2 days with 2 ng mL^{-1} of TGFβ before being plated on micropatterned PA substrates. As expected,[49] cells exhibited a significantly higher level of cell contraction as revealed by crossbow shortening (Fig. 5c). Interestingly, we found no significant changes in the level of cell contraction upon ErbB2 receptor activation (Fig. 5c). More surprisingly, in CK2b knockdown cells, the contraction level was significantly lower than in WT cells (Fig. 5c). These results show that different treatments, all inducing tumoral-like phenotypes, could either promote or reduce the level of cell contraction. They also demonstrate that our method can easily be used at larger scale to more precisely characterize this complex correlation between cell contraction and tumoral transformation.

Discussion

The use of deep UV exposure on PA in contact with the photomask is, to our knowledge, the most robust and easiest method to create homogeneous and reproducible micropatterns on soft deformable substrates. It allows a homogenous coating of ECM proteins over large micropatterned surfaces. In addition, it is faster than previous methods since it does not require any preliminary microfabrication step. These characteristics allowed this method to be adapted for large-scale production of soft micropatterned substrates. Considering the need to combine geometrical and mechanical control of cell microenvironment to recapitulate actual *in vivo* conditions for cell anchoring, we believe this new protocol will have a broad range of applications from fundamental research to tissue engineering.

The actin network streamlining and force field normalization in response to an appropriate micropattern geometry allow a precise calibration of the relationship between micropattern shape deformation and total traction forces. Thanks to the observed linear relationship between force and deformation, force measurement is simply obtained by measuring micropattern length. Classical force measurement methods are still required to obtain the calibration curve. However, afterwards, a single image acquisition is sufficient to measure micropattern length and read the corresponding traction force. The sensitive and difficult step of gel-embedded beads imaging and tracking is no longer required. Therefore, force measurement is as simple as the use of micropillars[9] without the microfabrication constraint. However since we do not consider micron-sized substrate deformations the spatial resolution is lower than the resolution that can be achieved with bead tracking.[32,50] Our method is adapted to provide an easy and fast measurement of the global

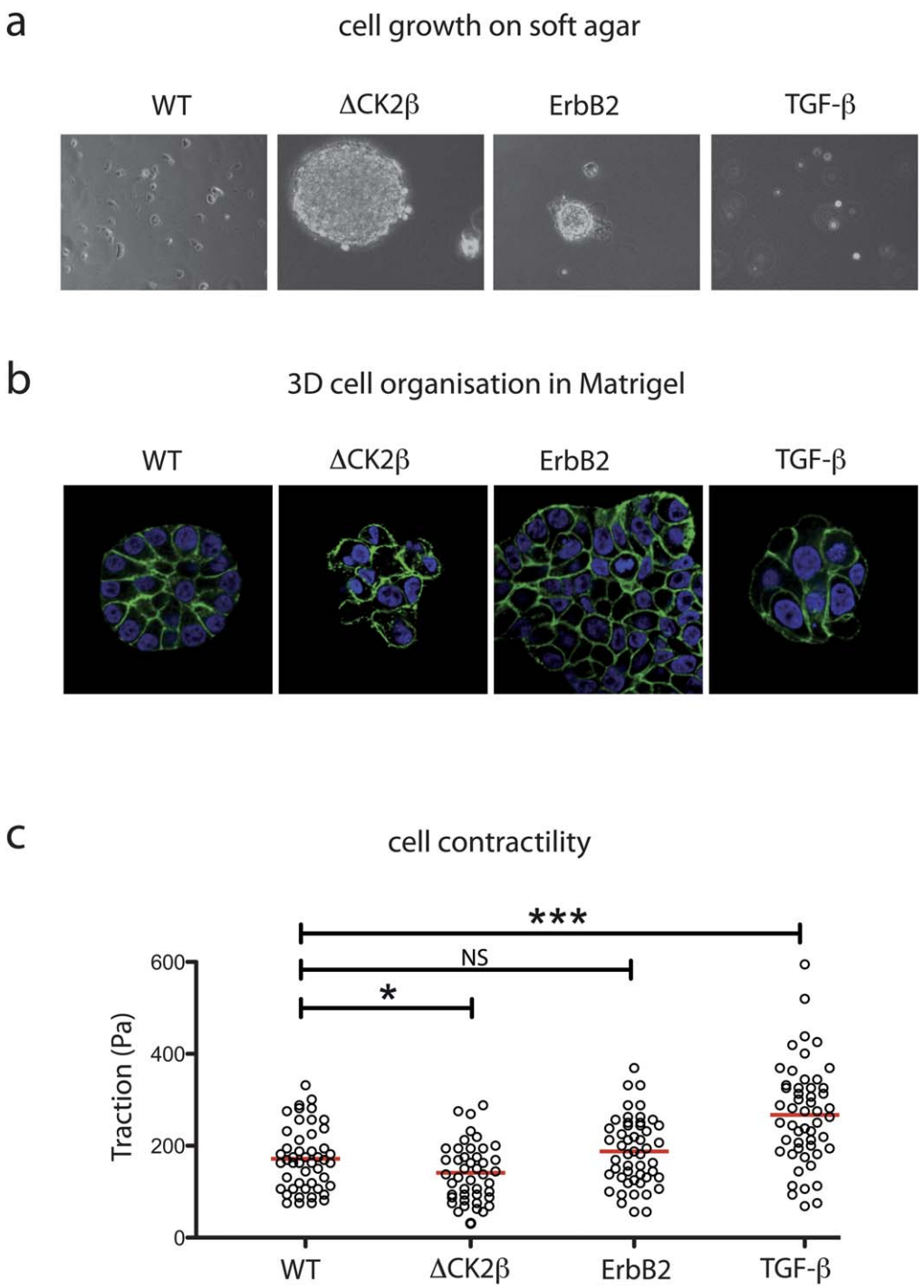

Fig. 5 Applications of large-scale force measurements to tumoral-like phenotypes. (a) Anchorage-independent growth. Cells were cultured on soft agar and imaged by phase contrast microscopy. Wild type cells died after a few days as revealed by the presence of black phantoms. CK2b knockdown cells and ErbB2 activated cells managed to grow in the absence of anchorage. TGFb1 treated cells form small aggregates (bright in phase contrast) and survived. (b) Self-assembly of 3D acini-like structures. Cells were cultured in Matrigel and stained for DNA (blue) and actin (green). Wild type cells formed spherical hollow structures as revealed by the low number of nuclei in the central part of the acini. CK2b knockdown cells, ErbB2 activated cells and TGFβ treated cells form irregular aggregates with mis-positioned cells in the central part of the structure. Pictures are 50 μm wide. (c) Cell traction forces calculated by the method illustrated in Fig. 3f in mutant or drug treated MCF10A cells mimicking tumor transformation. MCF10A WT cells were compared to CK2b knockdown cells, ErbB2 activated cells and TGFβ treated cells. Comparison between two sets of measures were performed using a student T test: two tailed, 95% interval confidence: * = $P < 0.05$ ** = $P < 0.01$ *** = $P < 0.001$.

cell contraction level with only a simple local measurement. In addition, it is easily amenable to automation since cell position and subcellular localization of force production are precisely controlled. This method paves the way to large scale and high throughput analysis of cell contraction state.

Our initial work identified characteristic tumoral-like phenotypes that were not associated to an increased level of cell contractility. High levels of contractility were observed in epithelial cells forming disorganized multicellular structures[21] or detaching from each others.[51] Such phenotypes are characteristic of advanced or late stages of tumoral transformation. ErbB2 receptor activation is a feature of early tumoral transformation that impacts on growth rate.[38] CK2 is also implicated in anti-apoptotic effect and CK2beta knockdown, specifically affecting p53-dependent cell survival.[41] Although contractility activates cell growth, early phases of cancer progression involving cell growth stimulation might not systematically be associated to a high level of contractility. It would be now necessary to more specifically analyze cell contraction levels at various phases of tumoral transformation to clarify the relationship between cancer progression and cell contraction. Mechanical property characterization of healthy and transformed cells could then be used to set up a new medical diagnosis test. Note that measurements have been performed on gels whose rigidity was about 7 kPa, but the relative levels of cell contractions for each treatment could have been different for another matrix rigidity.[52]

Conclusion

We developed a new method to micropattern poly-acrylamide gels. It associates the control of cell shape and microenvironment stiffness. This method could have a broad range of application notably in the design of new biomaterials for tissue engineering purpose. It can also be applied to the quantification of global cell contraction levels *via* the simple measurement of micropattern deformation. Our results suggested that not all cancer cells are more contracted than normal cells and that cell contraction levels may vary depending on the nature of the tumorigenic signal or the stage of cancer progression.

Experimental

PA micropatterning

25 mm round glass coverslips were first cleaned with piranha for 2 h and silanized by dipping in ethanol solution containing 2% (v/v) 3-(trimethoxysilyl)propyl methacrylate (Sigma) and 1% (v/v) acetic acid for 5 min. After cleaning with ethanol to remove excess silane residue, the coverslips were incubated at 120 °C for one hour.

Carboxylate modified polystyrene fluorescent beads (dark red 200 nm, Invitrogen F-8807) were passivated by poly(ethylene) glycol as follows: fluorescent beads were diluted 25-fold in MES buffer (10 mM pH 5.5) containing 8 mg mL^{-1} *N*-hydroxysuccinimide (NHS; Fluka) and 4 mg mL^{-1} EDC (1-ethyl-3-[3-dimethylaminopropyl]carbodiimide hydrochloride; Pierce) before 1 : 1 mixing with PLL-PEG (PLL(20)-g[3.5]-PEG(2); Susos) solution (4 mg mL^{-1} in 10 mM pH8.5 HEPES buffer). The mixture was incubated with rotation at 4 °C overnight. The beads were subsequently spun down and resuspended in HEPES buffer (10 mM pH 7.4).

The photomask was cleaned by *n*-hexane prior to use in order to maintain an hydrophobic surface. An acrylamide solution containing 6.67% acrylamide and 0.167% bis-acrylamide was mixed with passivated fluorescent beads by sonication before addition of APS and TEMED. A 35 μL drop of acrylamide solution was put directly on the chromium side of the photomask (Toppan). A silanized coverslip was placed over the drop and let it polymerize for 45 min. The sandwich was then exposed to deep UV in a UV–Ozone cleaner (Jelight) for 4 min. The coverslip, with gel, was carefully removed from the mask and incubated with 10 mg mL^{-1} EDC and 17 mg mL^{-1} NHS water solution for 15 min, and then coated with 20 ug mL^{-1} fibronectin (Sigma) and 5 μg mL^{-1} Alexa546 conjugated fibrinogen (Invitrogen) in HEPES buffer (10 mM pH 8.5) for one hour. The photomask was washed with water and then isopropanol. The gel was washed three times by PBS before seeding cells.

AFM measurement of micropatterned PA elasticity

All atomic force microscopy (AFM) measurements were carried out in PBS using a PicoPlus AFM (Agilent Technologies, USA). The spring constant of each cantilever was determined using the thermal noise method.[53] Force-indentation profiles were recorded using borosilicate sphere-tipped cantilevers with a radius, *R*, of 2.5 μm (Bioforce Nanoscience, IA, USA) and a spring constant of 60 mN m^{-1}. To delimitate insolated and non-insolated zones, topographies of 60 × 60 μm^2 were first imaged in contact mode with 512 × 512 $pixels^2$ at line rates of 0.5 Hz and with the same cantilevers. The sphere probe was then moved above the zone of interest before indentation. Young's moduli were calculated by least-square fitting of the experimental force-indentation curves. The measured Young modulus of UV exposed regions was 7.29 ± 0.42 kPa. The measured Young modulus of non-exposed regions was 6.64 ± 0.59 kPa.

Cell culture and treatments

The culture of MCF10A cells and the generation of ΔCK2β cell line was described previously.[40] The MCF10A cell expressing ligand inducible ErbB2 receptors were obtained from Ariad Pharmaceuticals.[38] Cells were seeded on the micro-patterned substrate at a density of 8×10^4 cm^{-2}. Cells not attaching to the adhesive region on the substrate were washed away 1–2 h after seeding. All the traction force measurements were performed 6 h after seeding to ensure a full spreading of the cells. Substrate relaxation was assessed by detaching cells with trypsin. To induce an ErbB2 cell line, AP1510 (Ariad Pharmaceuticals) was added to the culture medium to a final concentration of 1 μM, 48 h before traction force measurement.[38] TGFβ (R&D systems) was added at 2 ng mL^{-1} to the culture medium 48 h before cell plating on micropatterned PA and traction force measurement. Blebbistatin(-) (Sigma) at 100 μM was added progressively to the observation chamber to gradually obtain the specific final concentration for the drug dose-response experiment. While for the time response experiment, blebbistatin was added to directly reach a final concentration of 100 μM. Image acquisition started directly after the drug addition.

Anchorage-independent growth

Cells were detached with trypsin and resuspended in growth medium. Plates were prepared with a coating of 0.75% agarose (Cambrex) in growth medium and then overlaid with a suspension of cells in 0.45% agarose (5×10^3 cells per well). Plates were incubated for 4 weeks at 37 °C and colonies were imaged under a microscope.

Self-organization in 3D matrix

Cells (10 000) were seeded in chamber slides coated with growth factor reduced EHS ECM (Matrigel® BD Biosciences; with protein concentrations between 9 and 11 mg mL^{-1}) in assay medium (DMEM/F12 supplemented with 2% donor horse serum, 10 μg mL^{-1} insulin, 0.5 μg mL^{-1} hydrocortisone, 100 ng mL^{-1} cholera toxin, 5 ng mL^{-1} EGF (Peprotech, France). The assay medium was replaced every 3 days. When indicated, at day 6, cells were treated with 2 ng mL^{-1} TGFβ for 50 h.

Fixation and immuno-stainings

Six hours after seeding on the micropatterned gel or glass coverslip, the cells were first extracted in cytoskeleton buffer (10 mM MES, 138 mM KCl, 3 mM MgCl, 2 mM EGTA, pH 6.1) containing 0.5% Triton X-100, then fixed in 4% paraformaldehyde. 3D cell structures were fixed in 2% PFA, permeabilized in 0.5% Triton X-100–PBS. Fixed samples were wash 3 times in PBS. Afterward, samples were incubated for 1 h in PBS containing 0.1% Tween, 3% BSA, and 10 μM Phalloidin-FITC (Sigma) to stain actin filaments. On glass slides, cells were immuno labelled with primary antibodies directed against paxillin (BD Tranduction Laboratories) followed by immunolabelling with secondary Cy3-labelled antibodies (Jackson Immuno Research). All coverslips were stained with Hoechst 33342 (Sigma) to reveal cell nuclei for counting. After PBS washing, coverslips were mounted in Mowiol mounting medium.

Microscopy and Image processing

Images of fixed cells were taken with a 100× objective (NA = 1.35) on an Olympus BX-61 straight microscope, mounted with a CDD camera (HQ2, Ropper Scientific) and driven with Metamorph (Molecular Devices). Images of the 3D cell structures were performed using a Leica TCS-SP2 laser scanning confocal apparatus coupled to a Leica DMIRBE microscope. Live imaging of bead displacement and micropattern deformation were performed with a 63× objective (NA = 1.4) on an inverted 200 M Zeiss microscope, mounted with a CDD camera (HQ2, Ropper Scientific) and driven with Metamorph (Molecular Devices). Temperature and CO_2 control were ensured by the Cube and the Box from LIS Imaging.

All the acquired images were processed by ImageJ (http://rsb.info.nih.gov/ij/). Averaged fluorescent staining images were automatically aligned using micropattern images by a custom written plugin (https://sites.google.com/site/qingzongtseng/template-matching-ij-plugin). Pattern detection and length measurement were done automatically by custom written macro routines.

Traction force microscopy

Displacement fields describing the deformation of the PA substrate are determined from the analysis of fluorescent beads images before and after removal of the adhering cells with trypsin treatment. The displacement field is obtained by a two-step method consisting of particle image velocimetry followed by individual bead tracking.[32,33] A special procedure is used to evaluate displacements in the area of the adhesive pattern where gel deformation is expected to be largest. Depending on the pattern shape, traction forces may be strongly localized leading to large displacements in very small areas. In this case, failure to correctly track a few beads in such areas would significantly alter the calculated force magnitude. Therefore, the pattern area is divided into smaller windows that are allowed to overlap, before applying the cross-correlation and tracking analysis. Reducing the size of the windows makes it possible to retrieve larger displacements with cross-correlation and, using overlapped windows, we can avoid missing beads close to the windows boundaries. All image processing and analysis were performed using Matlab.[54]

To calculate cell-induced traction stress from displacement data, we have used the Fourier-transform traction cytometry (FTTC) method.[32,33] We kept the regularization parameter at small values ($\lambda < \sim 10^{-9}$) in order to maintain the best spatial resolution, which is estimated to be about 5 μm in our case.

Acknowledgements

We would like to thank Thomas Boudou, Catherine Picart, Claude Verdier and Michael Betton for AFM measurements of gel rigidities, as well as Alexandre Deshière and Laurent Blanchoin for interesting discussions. This work was supported by grants from Agence National pour la Recherche to OF and MT (ANR-PCV08_322457), from the CNRS (appel à prise de risques) to MB, from the fondation nanosciences RTRA to MB and from the Université Joseph Fourier (program SMING) to MB and MT.

References

1 M. Thery, *J Cell Sci*, 123, pp. 4201–4213.
2 D. Falconnet, G. Csucs, H. M. Grandin and M. Textor, *Biomaterials*, 2006, **27**, 3044–3063.
3 H. B. Wang, M. Dembo and Y. L. Wang, *Am. J. Physiol. -Cell Physol.*, 2000, **279**, C1345–C1350.
4 G. Blin, N. Lablack, M. Louis-Tisserand, C. Nicolas, C. Picart and M. Puceat, *Biomaterials*, 2010, **31**, 1742–1750.
5 V. Damljanovic, B. C. Lagerholm and K. Jacobson, *BioTechniques*, 2005, **39**, 847–851.
6 N. Wang, E. Ostuni, G. M. Whitesides and D. E. Ingber, *Cell Motil. Cytoskeleton*, 2002, **52**, 97–106.
7 K. K. Parker, A. L. Brock, C. Brangwynne, R. J. Mannix, N. Wang, E. Ostuni, N. A. Geisse, J. C. Adams, G. M. Whitesides and D. E. Ingber, *FASEB J.*, 2002, **16**, 1195–1204.
8 A. J. Engler, M. A. Griffin, S. Sen, C. G. Bonnemann, H. L. Sweeney and D. E. Discher, *J. Cell Biol.*, 2004, **166**, 877–887.
9 J. L. Tan, J. Tien, D. M. Pirone, D. S. Gray, K. Bhadriraju and C. S. Chen, *Proc. Natl. Acad. Sci. U. S. A.*, 2003, **100**, 1484–1489.
10 M. Théry, A. Pepin, E. Dressaire, Y. Chen and M. Bornens, *Cell Motil. Cytoskeleton*, 2006, **63**, 341–355.
11 A. J. Engler, S. Sen, H. L. Sweeney and D. E. Discher, *Cell*, 2006, **126**, 677–689.
12 J. Fu, Y. K. Wang, M. T. Yang, R. A. Desai, X. Yu, Z. Liu and C. S. Chen, *Nat. Methods*, 2010, **7**, 733–736.

13 V. Chevrier, M. Piel, N. Collomb, Y. Saoudi, R. Frank, M. Paintrand, S. Narumiya, M. Bornens and D. Job, *J. Cell Biol.*, 2002, **157**, 807–817.
14 A. Pitaval, Q. Tseng, M. Bornens and M. Théry, *J. Cell Biol.*, 2010, **191**, 303–312.
15 S. Miserey-Lenkei, G. Chalancon, S. Bardin, E. Formstecher, B. Goud and A. Echard, *Nat. Cell Biol.*, 2010, **12**, 645–654.
16 W. Yu, A. M. Shewan, P. Brakeman, D. J. Eastburn, A. Datta, D. M. Bryant, Q. W. Fan, W. A. Weiss, M. M. Zegers and K. E. Mostov, *EMBO Rep.*, 2008, **9**, 923–929.
17 C. M. Lo, D. B. Buxton, G. C. Chua, M. Dembo, R. S. Adelstein and Y. L. Wang, *Mol. Biol. Cell*, 2004, **15**, 982–989.
18 A. D. Doyle, F. W. Wang, K. Matsumoto and K. M. Yamada, *J. Cell Biol.*, 2009, **184**, 481–490.
19 A. S. Maddox and K. Burridge, *J. Cell Biol.*, 2003, **160**, 255–265.
20 E. A. Klein, L. Yin, D. Kothapalli, P. Castagnino, F. J. Byfield, T. Xu, I. Levental, E. Hawthorne, P. A. Janmey and R. K. Assoian, *Curr. Biol.*, 2009, **19**, 1511–1518.
21 M. J. Paszek, N. Zahir, K. R. Johnson, J. N. Lakins, G. I. Rozenberg, A. Gefen, C. A. Reinhart-King, S. S. Margulies, M. Dembo, D. Boettiger, D. A. Hammer and V. M. Weaver, *Cancer Cell*, 2005, **8**, 241–254.
22 J. M. Vasiliev, T. Omelchenko, I. M. Gelfand, H. H. Feder and E. M. Bonder, *Proc. Natl. Acad. Sci. U. S. A.*, 2004, **101**, 12526–12530.
23 K. P. Landsberg, R. Farhadifar, J. Ranft, D. Umetsu, T. J. Widmann, T. Bittig, A. Said, F. Julicher and C. Dahmann, *Curr. Biol.*, 2009, **19**, 1950–1955.
24 M. Rauzi, P. Verant, T. Lecuit and P. F. Lenne, *Nat. Cell Biol.*, 2008, **10**, 1401–1410.
25 S. Huang, C. S. Chen and D. E. Ingber, *Mol. Biol. Cell*, 1998, **9**, 3179–3193.
26 F. Rehfeldt, A. J. Engler, A. Eckhardt, F. Ahmed and D. E. Discher, *Adv. Drug Delivery Rev.*, 2007, **59**, 1329–1339.
27 A. J. Ridley, *Breast Cancer Res. Treat.*, 2004, **84**, 13–19.
28 A. Welle and E. Gottwald, *Biomed. Microdevices*, 2002, **4**, 33–41.
29 S. A. Mitchell, A. H. C. Poulsson, M. R. Davidson, N. Emmison, A. G. Shard and R. H. Bradley, *Biomaterials*, 2004, **25**, 4079–4086.
30 A. Azioune, M. Storch, M. Bornens, M. Thery and M. Piel, *Lab Chip*, 2009, **9**, 1640–1642.
31 W. A. Marganski, M. Dembo and Y. L. Wang, *Methods Enzymol.*, 2003, **361**, 197–211.
32 B. Sabass, M. L. Gardel, C. M. Waterman and U. S. Schwarz, *Biophys. J.*, 2008, **94**, 207–220.
33 J. P. Butler, I. M. Tolic-Norrelykke, B. Fabry and J. J. Fredberg, *Am. J. Physiol. -Cell Physol.*, 2002, **282**, C595–605.
34 A. Straight, A. Cheung, J. Limouze, I. Chen, N. Westwood, J. Sellers and T. J. Mitchison, *Science*, 2003, **299**, 1743–1747.
35 D. Mitrossilis, J. Fouchard, A. Guiroy, N. Desprat, N. Rodriguez, B. Fabry and A. Asnacios, *Proc. Natl. Acad. Sci. U. S. A.*, 2009, **106**, 18243–18248.
36 D. T. Butcher, T. Alliston and V. M. Weaver, *Nat. Rev. Cancer*, 2009, **9**, 108–122.
37 J. Massague, *Cell*, 2008, **134**, 215–230.
38 S. K. Muthuswamy, D. Li, S. Lelievre, M. J. Bissell and J. S. Brugge, *Nat. Cell Biol.*, 2001, **3**, 785–792.
39 M. R. MacPherson, P. Molina, S. Souchelnytskyi, C. Wernstedt, J. Martin-Perez, F. Portillo and A. Cano, *Mol. Biol. Cell*, 2009, **21**, 244–253.
40 A. Deshiere, N. Theis-Febvre, V. Martel, C. Cochet and O. Filhol, *Mol. Cell. Biochem.*, 2008, **316**, 107–113.
41 V. Martel, O. Filhol, P. Colas and C. Cochet, *Oncogene*, 2006, **25**, 7343–7353.
42 M. Ruzzene and L. A. Pinna, *Biochim. Biophys. Acta, Proteins Proteomics*, 2010, **1804**, 499–504.
43 J. H. Trembley, G. Wang, G. Unger, J. Slaton and K. Ahmed, *Cell. Mol. Life Sci.*, 2009, **66**, 1858–1867.
44 N. H. Colburn, W. F. Bruegge, J. R. Bates, R. H. Gray, J. D. Rossen, W. H. Kelsey and T. Shimada, *Cancer Res.*, 1978, **38**, 624–634.
45 P. J. Reddig and R. L. Juliano, *Cancer Metastasis Rev.*, 2005, **24**, 425–439.
46 J. Debnath and J. S. Brugge, *Nat. Rev. Cancer*, 2005, **5**, 675–688.
47 M. K. Wendt, J. A. Smith and W. P. Schiemann, *Oncogene*, 2010, **29**, 6485–6498.
48 J. Debnath, S. K. Muthuswamy and J. S. Brugge, *Methods*, 2003, **30**, 256–268.
49 J. Chen, H. Li, N. SundarRaj and J. H. Wang, *Cell Motil. Cytoskeleton*, 2007, **64**, 248–257.
50 J. Stricker, B. Sabass, U. S. Schwarz and M. L. Gardel, *J. Phys.: Condens. Matter*, 2010, 22.
51 J. de Rooij, A. Kerstens, G. Danuser, M. A. Schwartz and C. M. Waterman-Storer, *J. Cell Biol.*, 2005, **171**, 153–164.
52 R. W. Tilghman, C. R. Cowan, J. D. Mih, Y. Koryakina, D. Gioeli, J. K. Slack-Davis, B. R. Blackman, D. J. Tschumperlin and J. T. Parsons, *PLoS One*, 2010, **5**, e12905.
53 H. J. Butt and M. Jaschke, *Nanotechnology*, 1995, **6**, 1–7.
54 Y. X. Gao and M. L. Kilfoil, *Opt. Express*, 2009, **17**, 4685–4704.

